AIRBRAKE INDUCED FIN BUFFET LOADS ON FIGHTER AIRCRAFT

Christian Breitsamter
Institute of Aerodynamics, Technische Universität München
Boltzmannstrasse 15, D-85748 Garching, Germany

Keywords: *Vortex flows, high agility aircraft, unsteady loads, fin buffeting, airbrake*

Abstract

The investigations presented focus on the influence of an airbrake wake on the buffet characteristics of the vertical tail (fin) of a single-finned high-agility aircraft. The study uses a detailed wind tunnel model of a delta-canard configuration fitted with a center-line airbrake located at the rear part of the canopy. The results include turbulent flowfield data based on advanced hot-wire anemometry as well as unsteady fin surface pressures measured with integrated sensors. The tests are conducted in the low-speed region at Reynolds number $Re_{l\mu} \approx 1 \times 10^6$ for an angle-of-attack range of $\alpha = 0° - 30°$ and two airbrake deflection angles of $\eta_{AB} = 45°$ and 60°. The airbrake near field wake shows specific turbulent flow structures associated with the flow separation at the airbrake side edges and upper edge. Vortices are formed which are orientated vertically or axially depending on the angle of attack. The corresponding region of high turbulence intensities impinges on the fin while the turbulence levels in the center area increase with angle of attack. This increase is caused by the inboard movement and expansion of the wing and canard leading-edge vortices compressing the airbrake wake in the fin area. At low angles of attack, the airbrake wake exhibits concentrations of turbulent kinetic energy at characteristic frequencies attributed to the airbrake vortex shedding. At high angles of attack, the fin is also subject to quasi-periodic aerodynamic loads evoked by induction of the breakdown flow of the wing vortices.

1 Introduction

The flight envelope of high maneuverable aircraft is limited by dynamic aeroelastic problems like buffeting, buzz and flutter [1-3]. Especially, the fin buffeting problem is a critical issue for high performance fighter aircraft equipped with twin vertical tails [4], but single fin configurations are also affected [5, 6]. The associated unsteady aerodynamic loads occur mainly at high angles of attack and are attributed to the highly turbulent flow caused by burst leading-edge vortices. Strong large-scale vortices are shed at slender wing geometries, such as delta wing planforms, strakes or leading-edge extensions [7, 8]. Leading-edge vortices in a fully developed, stable stage improve significantly maneuver capabilities because of additional lift and an increase in maximum angle of attack. However, leading-edge vortices are subject to breakdown at high angles of attack [9, 10]. The breakdown flow leads to high turbulence levels and specific instability mechanisms resulting in narrow-band unsteady aerodynamic forces [6, 11, 12]. Such loads often excite the vertical tail structure in its natural frequencies (Fig. 1) causing increased fatigue loads and reduced service life and raise maintenance costs [13]. Comprehensive studies concentrate on the fin buffeting problem including also methods for flow control and active vibration alleviation [14, 15].

Beside the unsteady effects linked with burst leading-edge vortices, further configuration elements like airbrakes produce also high energy turbulent wakes which may cause severe fin buffet loads. The superposition of unsteady loads due to wing vortex breakdown flow and airbrake wake could result in critical peak loads.

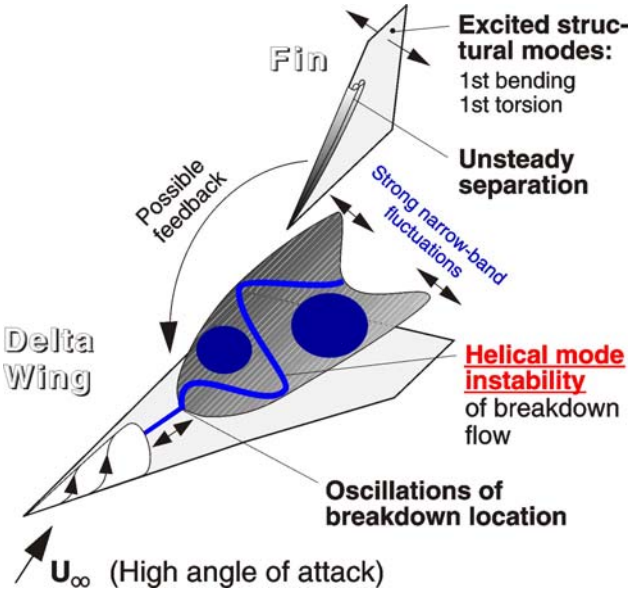

Fig. 1 Phenomenology of fin buffeting induced by the flow of burst leading-edge vortices.

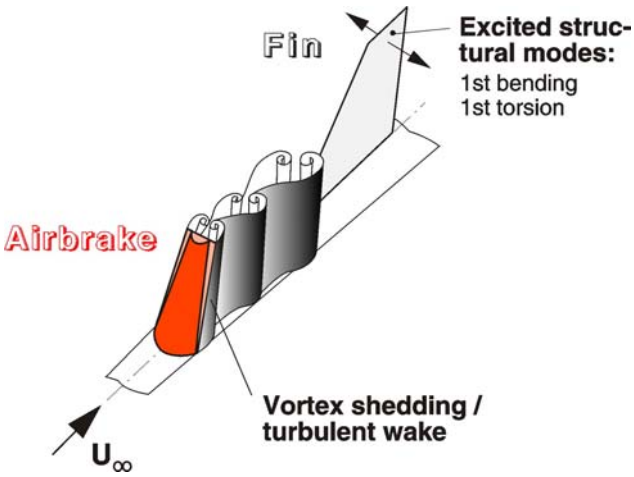

Fig. 2 Phenomenology of fin buffeting evoked by turbulent wakes shed at bluff bodies.

There are a lot of investigations dealing with the turbulent wake of bluff bodies [16 – 19], but no studies address the effects in combination with lifting surfaces creating leading-edge vortices.

Therefore, the present investigation concentrates on the analysis of the turbulent velocity fields and fin surface pressures downstream of a deflected airbrake on a delta wing-canard configuration. Vortex shedding at the airbrake side edges and the upper edge will result in strong periodic fluctuations affecting the fin (Fig. 2). Thus, the main investigation parameters include airbrake deflection angle and angle of attack.

2 Experimental Technique

2.1 Model and Facility

Experiments are performed on an 1:15 scaled detailed steel model of a modern high-agility aircraft of canard-delta wing type (Fig. 3a). Major parts of the model are nose section, front fuselage with rotatable canards and a single place canopy, center fuselage with delta wing and a through-flow double air intake underneath, and rear fuselage including nozzle section and vertical tail (fin).

The airbrake is located in the rear part of the canopy with a length of 0.36 and a width of 0.14 based on the wing half span. The airbrake model consists of the deflected canopy fairing and the actuator sting (Fig. 3b). Because of the sharp side and upper edges of the airbrake it is assumed that flow separation is only little influenced by direct boundary layer effects. The airbrake deflection angles studied include η_{AB} = 45°, and 60°.

The experiments have been carried out in the low-speed facility B of the Institute of Aerodynamics of Technische Universität München. This closed-return wind tunnel is operated with an open test section at maximum usable velocity of 60 *m/s*. Test section dimensions are 1.2 *m* in height, 1.55 *m* in width and 2.8 *m* in length. The test section flow was carefully inspected and calibrated documenting a turbulence level less than 0.4% and uncertainties in the spatial and temporal mean velocity distributions of less than 0.067%. The maximum blockage at the model incidence of $\alpha = 30°$ is about 6%.

The model is sting mounted using a Z-shape adapter for connection with the horizontal sting of the 3-axis model support (Fig. 3c). The computer controlled model support provides an angle-of-attack range of $-10° \leq \alpha \leq +30°$, and models may be yawed and rolled 360°. The uncertainty in angle setting is less than 0.05°.

2.1 Test Methods and Test Conditions

The fin is instrumented with 18 differential unsteady pressure transducers at 9 positions directly opposite each other on each surface. The

2s	= 0.740 m,	φ_W	= 50°	Indices:
l_μ	= 0.360 m,	φ_C	= 45°	W: Wing
Λ_W	= 2.45,	λ_W	= 0.14	C: Canard
Λ_F	= 1.38,	φ_F	= 54°	F: Fin

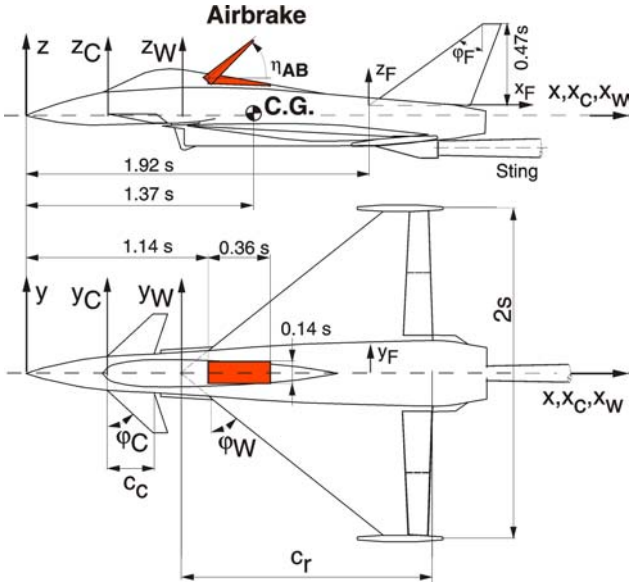

a) Geometry and reference quantities

b) Airbrake model

c) Model mounted in the test section

Fig. 3 Delta-canard configuration.

sensor voltages of each channel are amplified for optimal signal levels, low-pass filtered at 256 *Hz* and sampled with 2000 *Hz*. The data of all channels are acquired simultaneously over a time interval of 30 *sec*. and digitized with 14 bit precision. The signal resolution is about 2 *Pa*.

The time dependent flowfield velocities are measured using advanced hot-wire anemometry. A 3-axes traversing system moves a miniature cross-wire probe to the points of four cross-flow planes located downstream of the airbrake above the fuselage (Fig. 4). The spacing of the measurement points based on the wing half span is 0.013 in the inner and 0.027 in the outer area of the cross-flow planes. The anemometer output voltages are low-pass filtered at 1000 *Hz* and sampled with 3000 *Hz* over 6.4 seconds. The data acquisition parameters are based on previous tests to ensure that all significant flowfield phenomena are captured as well as on statistical accuracies of 1%, and 2.5% for the root mean square (rms) values and spectral densities, respectively.

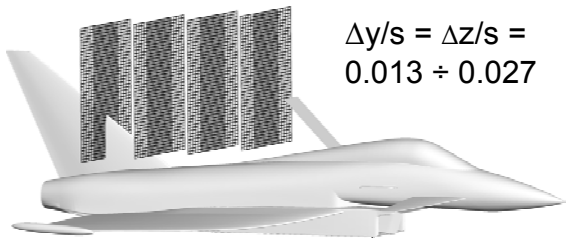

Fig. 4 Location of measured cross-flow planes and resolution of measurement grid.

The measurements have been made at a freestream reference velocity of U_∞ = 40 *m/s* at ambient pressure p_∞ and ambient temperature T_∞. The corresponding Reynolds numbers based on the wing mean aerodynamic chord l_μ is $Re_{l\mu} = 0.97 \times 10^6$. Thus, turbulent boundary layers are present at wing and control surfaces. All control surfaces, namely canard and leading- and trailing-edge flaps, are set to 0°. Flowfield surveys are conducted at angles of attack of α = 0°, 15°, and 20°, while fin pressure fluctuations are taken in the range of $0° \le \alpha \le 30°$ at an incidence step of $\Delta\alpha$ = 1°.

3 Results and Discussion

3.1 Baseline Configuration

The flowfield of the delta-canard configuration is characterized by the presence of leading-edge vortices. Such vortices start to develop at wing and canard already at low angles of attack. At $\alpha = 15°$, the wing leading-edge vortex is clearly depicted by the velocity vectors of the cross-flow planes located at 40% ($x/c_r = 0.4$) and 100% ($x/c_r = 1.0$) wing root chord (Fig. 5). Bursting of the wing leading-edge vortex occurs at $x/c_r \approx 0.4$ indicated by the enlarged core region of very low velocities.

Vortex breakdown is caused by the adverse pressure gradient leading to stagnation of the axial core flow. Consequently, the core diameter expands rapidly and high turbulence intensities exist at the points of inflection in the radial profiles of retarded axial core flow. Thus, an annular region of high velocity fluctuations surrounds the expanded vortex core. With increasing angle of attack the burst wing leading-edge vortices move inboard and upward with the core region being further strongly enlarged. Therefore, the areas of maximum turbulence intensities approach the symmetry plane and the turbulence level at the center-line fin raises from low to moderate levels at a steep gradient.

The unsteady flowfield induces pressure fluctuations on the fin. The surface-averaged rms values of the fluctuations in the pressure coefficient are plotted as function of angle of attack in Fig. 6. Representing the trend in the lateral turbulence intensities the rms pressure

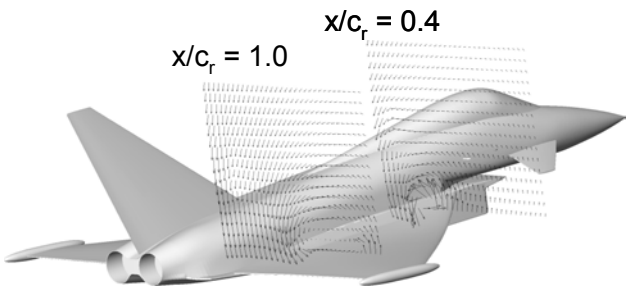

Fig. 5 Cross-flow velocity vectors at $x/c_r = 0.4$ and $x/c_r = 1.0$ at $\alpha = 15°$; $U_\infty = 40$ m/s, $Re_{l\mu} = 0.97 \times 10^6$.

coefficient increases significantly above $\alpha = 20°$ reaching a value of about 8% at maximum angle of attack of $\alpha \approx 30°$. The severe increase in the rms pressure above a certain incidence is a characteristic feature of the fin buffet phenomenon.

The amplitude spectra of the fluctuating pressure coefficient, calculated from the signal taken at station P13, are shown in Fig. 7 for all angles of attack tested. Above $\alpha \approx 22°$, spectral peaks can be identified in the range of reduced frequencies $k = 0.8 - 0.6$ ($k = f\, l_\mu / U_\infty$). This energy peak, called "buffet peak", increases strongly with increasing angle of attack. Thus, the narrow-band concentration of turbulent kinetic energy may result in strong excitation of structural modes. It can be further detected that the associated reduced frequencies are shifted to lower values at higher angle of attack.

This shift in the dominant reduced frequency is plotted in Fig. 8. The quasi periodic velocity and induced surface pressure fluctuations, respectively, result from the helical mode instability of the flow downstream of vortex breakdown. The burst vortex core expands with increasing angle of attack and, therefore, the wavelength of the instability mode becomes larger and the corresponding frequency smaller. A universal frequency parameter can be derived using appropriate scaling quantities. Referring to velocity, the component normal to the leading-edge ($U_\infty \sin\alpha$) has to be considered. The length scale must account for the vortex core expansion given approximately by the local half span ($\sim x \cot \varphi_W$) and the shear layer distance ($\sim \sin^2\alpha$). Using these relations leads to a scaling with the sinus of angle of attack α and the cotangent of the wing leading-edge sweep φ_W. This scaling groups the values of the dominant reduced frequencies within a band of 0.28 ± 0.02. Measurements on different configurations substantiates the validity of the derived frequency parameter [6, 11, 12].

3.2 Airbrake Configuration

In comparison to the baseline configuration, the flowfields for the cases of deflected airbrake are

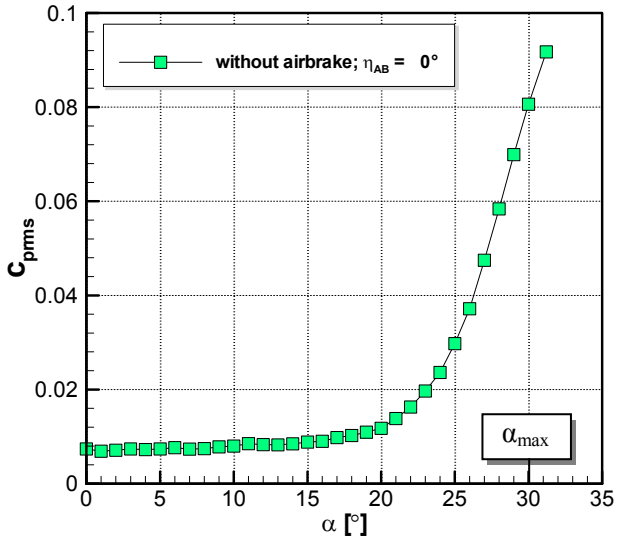

Fig. 6 Surface-averaged rms fin pressure coefficient c_{prms} as function of angle of attack α; U_∞ = 40 m/s, $Re_{l\mu}$ = 0.97 x 10^6.

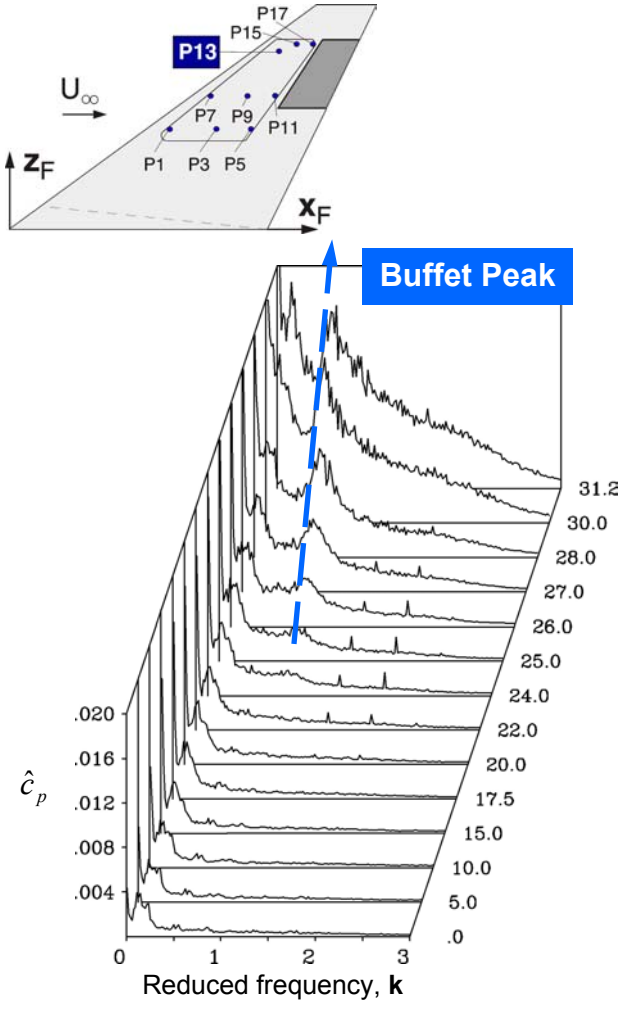

Fig. 7 Amplitude spectra of fluctuating fin surface pressure coefficient for station P13 at α = 0° - 31.2°; U_∞ = 40 m/s, $Re_{l\mu}$ = 0.97 x 10^6.

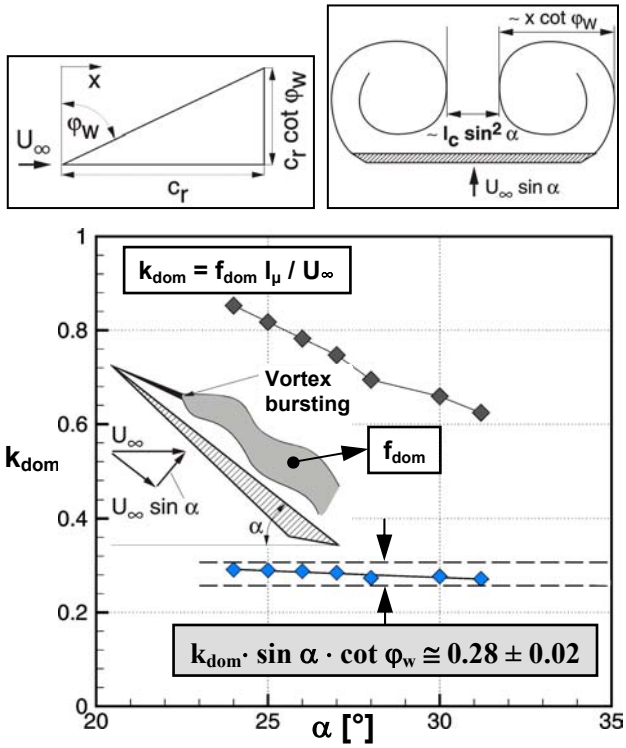

Fig. 8 Scaled dominant reduced buffet frequency k_{dom} as function of angle of attack based on amplitude pressure spectra of fin station P13.

analyzed showing specific phenomena superimposed to the baseline characteristics.

3.2.1 Mean and Turbulent Flowfield

The cross-flow velocity vectors give an overview of the mean flowfield development in the airbrake wake for stations close behind the airbrake and at the fin root (Fig. 9). Results are shown for both airbrake deflections, namely η_{AB} = 45° and 60°, and for angles of attack of α = 0° and 20°. The velocity components are based on a wind tunnel fixed coordinate system. For the upstream station, the mean velocities depict increased cross-flow components directed toward the dead water region behind the airbrake. In the lower part of the symmetry plane high cross flow velocities are present with their vectors pointing inboard und upward. Flow separation at the airbrake edges result in a counter rotating vortex pair which continue to exist downstream up to the fin region. A second vortex pair can be detected at the lower corners of the measurement planes associated with flow separation at the canopy (Fig. 9). The induced cross flow velocities, especially in the area above the fuse-

lage, increase in strength with increasing angle of attack, and the airbrake wake becomes laterally compressed. At α = 20°, a further vortex system dominates the lower outboard parts of the measurement planes. This vortex system consists of the canard leading- and side-edge vortices and both vortices are already bursted.

The discussion of the unsteady flowfield focuses on the turbulence intensity of the lateral velocity fluctuations v_{rms}/U_∞. The shear layers emanating from the upper edge and the side edges of the airbrake form a horseshoe-like region of increased turbulence intensities (Fig. 10). There, turbulence maxima occur in a limited radial range. At α = 10° and η_{AB} = 45°, the rms maxima reach levels of about 16% of the freestream velocity. Downstream, the inboard directed cross-flow velocities push the areas of turbulence maxima together. Thus, an annular region of high velocity fluctuations exists and determines the flowfield features in the symmetry plane at the fin location. Raising the airbrake deflection to η_{AB} = 60° enlarges the radial range of the region of increased turbulence intensities. This enlargement is also shown as a vertically extended area of maximum velocity fluctuations impinging on the fin. Beside this spatially extension, also higher turbulence levels are present.

The turbulence intensity distributions at α = 15° are included in Fig. 11. The canard vortex system reveals itself by circle-like areas of increased velocity fluctuations which are well separated from the airbrake wake. Donwstream, the cross-flow velocities induced by the canard vortices have the effect that the high turbulence intensity region at the fin is stretched in direction to the fuselage. In addition, this region is compressed because of the inboard and upward movement and the radial expansion of the burst wing vortices with increasing angle of attack. Consequently, the region of maximum turbulence intensities covers nearly the whole height of the fin at η_{AB} = 60°.

The influence of the canard and wing vortices becomes even stronger at α = 20° (Fig. 12). On the one hand, the velocity fluctuations attributed to the burst canard vortices raise the turbulence intensity level in the root area of the fin. On the other hand, the incidence dependent movement and expansion of the burst wing vortices compresses further the region of high turbulence intensities over the fin surface. Therefore, an absolute rms maximum is found near the fin tip reflecting a high excitation level.

Further, the airbrake wake exhibits specific frequency dependent concentrations of turbulent kinetic energy (Fig. 13, α = 0°). They result from coherent turbulent structures linked to quasi-periodic vortex shedding at the airbrake edges.

3.2.2 Pressure fluctuations on fin surface

The unsteady velocities induce pressure fluctuations on the fin which are again quantified by the surface averaged rms values of the fluctuating part of the pressure coefficient c_{prms} (Fig. 14). The reference is given by the results of the baseline configuration (Fig. 6). Compared to the baseline, the configurations with deflected airbrake, η_{AB} = 45° and 60°, show siginifcantly higher rms values up to α ≈ 25°. The pressure fluctuations on the fin surface become stronger with increased airbrake deflection. But the differences in rms pressures between both deflections are small for low and moderate angles of attack. Also, the rms levels are nearly constant up to α ≈ 12°. These features are based on the similarity of the airbrake wake flow with periodic vortex shedding and dominating cross flow.

For α > 12°, the decrease in effective airbrake deflection angle with increasing angle of attack becomes relevant. Thus, the vortex development changes from a vertical to a more axial orientation. In addition, the airbrake wake is strongly influenced by the expansion of the burst wing vortices and induction effects of the burst canard vortices. Consequently, the significant raise in rms pressures with angle of attack is shifted to lower α in comparison to the baseline, and it starts here at α ≈ 12°. At high angle of attack, α > 25°, the airbrake incidence becomes low through which vortex evolution at the side edges is stopped. The unsteady pressure characteristics follow then the trend of the baseline configuration. The pressure fluctuation intensities at certain sensor positions reach levels

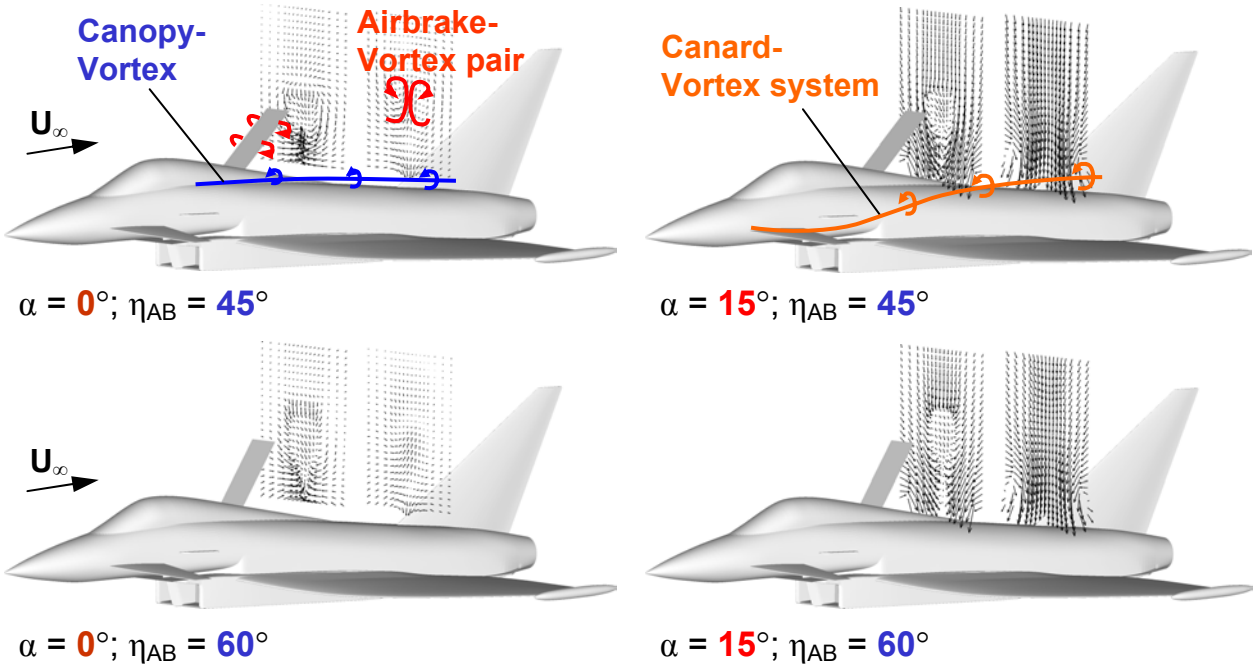

Fig. 9 Cross-flow velocity vectors for two planes in the airbrake wake at $\alpha = 0°$, and 15° and $\eta_{AB} = 45°$, and 60°; $U_\infty = 40$ m/s, $Re_{l\mu} = 0.97 \times 10^6$.

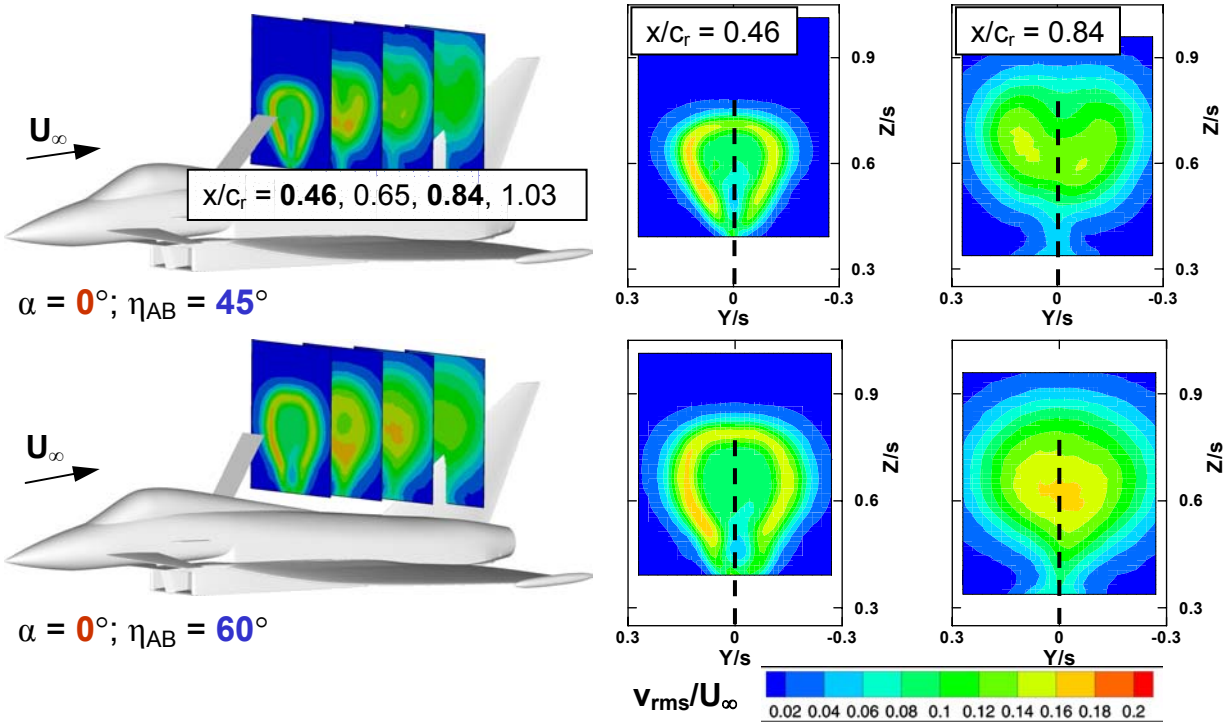

Fig. 10 Turbulence intensity distributions of the lateral velocity fluctuations v_{rms}/U_∞ for four cross-planes in the airbrake wake at $\alpha = 0°$ and $\eta_{AB} = 45°$, and 60°; $U_\infty = 40$ m/s, $Re_{l\mu} = 0.97 \times 10^6$.

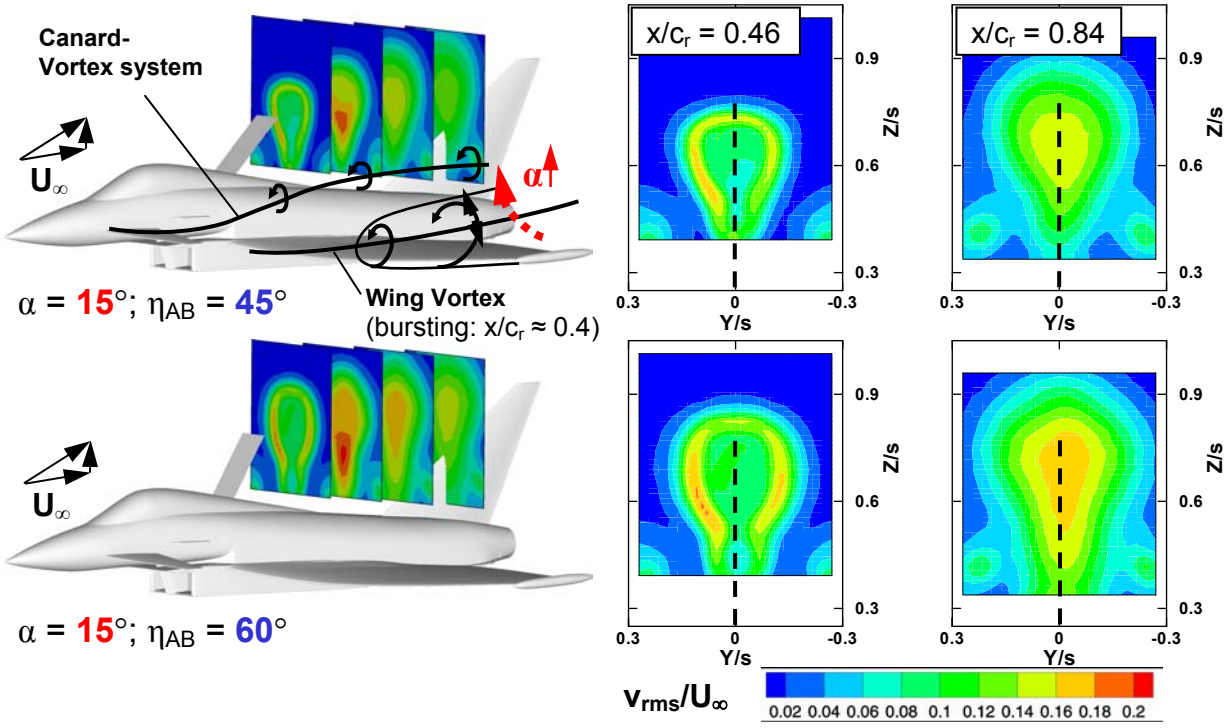

Fig. 11 Turbulence intensity distributions of the lateral velocity fluctuations v_{rms}/U_∞ for four cross-planes in the airbrake wake at $\alpha = 15°$ and $\eta_{AB} = 45°$, and 60°; $U_\infty = 40$ m/s, $Re_{l\mu} = 0.97 \times 10^6$.

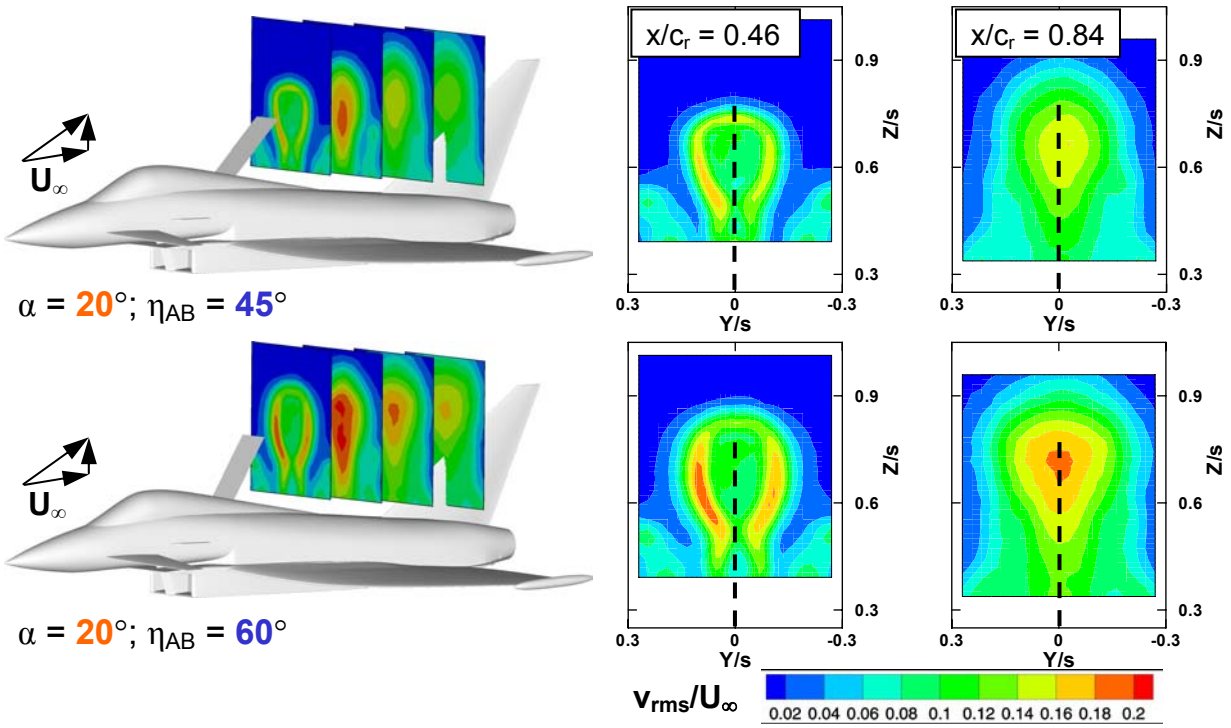

Fig. 12 Turbulence intensity distributions of the lateral velocity fluctuations v_{rms}/U_∞ for four cross-planes in the airbrake wake at $\alpha = 20°$ and $\eta_{AB} = 45°$, and 60°; $U_\infty = 40$ m/s, $Re_{l\mu} = 0.97 \times 10^6$.

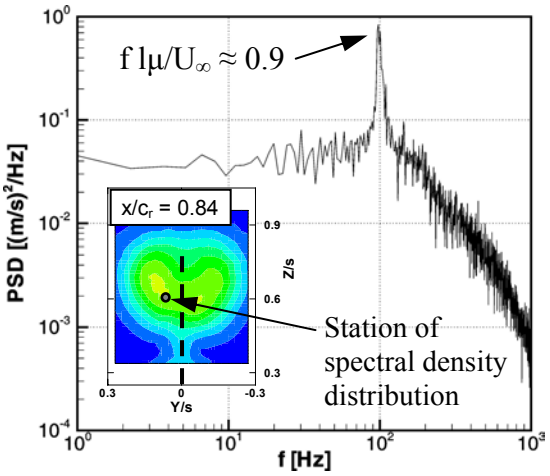

Fig. 13 Spetral density distribution of lateral velocity fluctuations at $x/c_r = 0.84$, $\alpha = 0°$ and $\eta_{AB} = 45°$; $U_\infty = 40$ m/s, $Re_{l\mu} = 0.97 \times 10^6$.

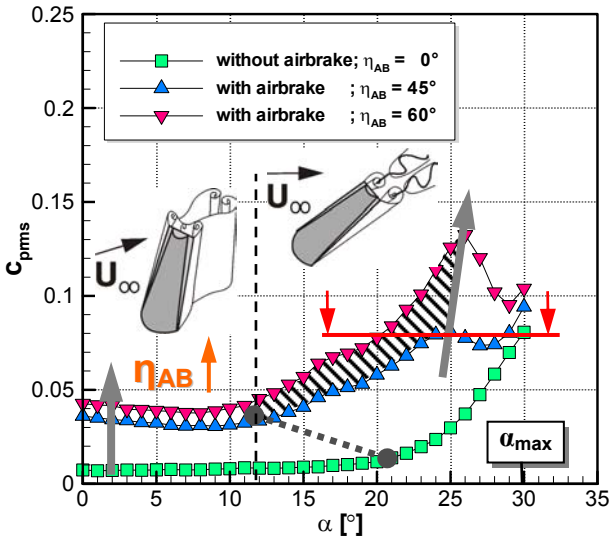

Fig. 14 Surface-averaged rms fin pressure coefficient c_{prms} as function of angle of attack α for airbrake deflections of $\eta_{AB} = 45°$, and 60°; $U_\infty = 40$ m/s, $Re_{l\mu} = 0.97 \times 10^6$.

which are two times higher than the surface averaged values. A reduction of the airbrake deflection from $\eta_{AB} = 60°$ to $\eta_{AB} = 0°$ within the angle-of-attack range of $\alpha = 20° - 25°$ avoids these peak values of surface pressure fluctuation intensities. It ensures that the dynamic loads do not exceed the limiting values of the baseline configuration given by maximum angle-of-attack conditions.

3.2.3 Characteristics of Reduced Frequencies

Beside the intensity of the pressure fluctuations, the frequency characteristics are of specific interest with respect to the excitation of structural modes. Power spectral densities (PSD's) of the surface pressure fluctuations are calculated to analyze narrow-band energy concentrations and to determine dominant reduced frequencies and angle-of-attack trends. Results are shown exemplarily for the sensor station P17 (Fig. 15).

At low and moderate angles of attack, here $\alpha = 3°$ and $\alpha = 10°$, the periodic vortex shedding results in strong spectral density peaks. The dominant reduced frequencies based on free-stream velocity and wing mean aerodynamic chord show higher values for $\eta_{AB} = 45°$ than for $\eta_{AB} = 60°$. For both cases, the reduced frequencies are nearly constant over the angle-of-attack range of $\alpha = 0° - 12°$, highlighting again the similarity of airbrake vortex shedding in this incidence range. This reduced frequency characteristic changes at $\alpha > 12°$ when airbrake side-edge vortices transform to leading-edge vortices due to the decrease in the side-edge inclination. The turbulent energy concentration is shifted to higher reduced frequencies the values of which increase with increasing angle of attack because the airbrake incidence becomes reduced. Beyond $\alpha \approx 25°$, the large-scale vortex evolution at the airbrake disappears and the helical mode instability of the burst wing vortices dominate the unsteady characteristics of the fin surface pressure fluctuations (Fig. 8).

An appropriate scaling with length scales including shear layer distances and the effective airbrake deflection and incidence, respectively, results in a common scaling parameter as documented in Fig. 16.

4 Conclusions and Outlook

Flowfield and surface pressure measurements were performed to study the influence of a deflected airbrake on the buffet characteristics of a vertical tail (fin). The results are based on wind tunnel studies conducted on an 1.15 scaled

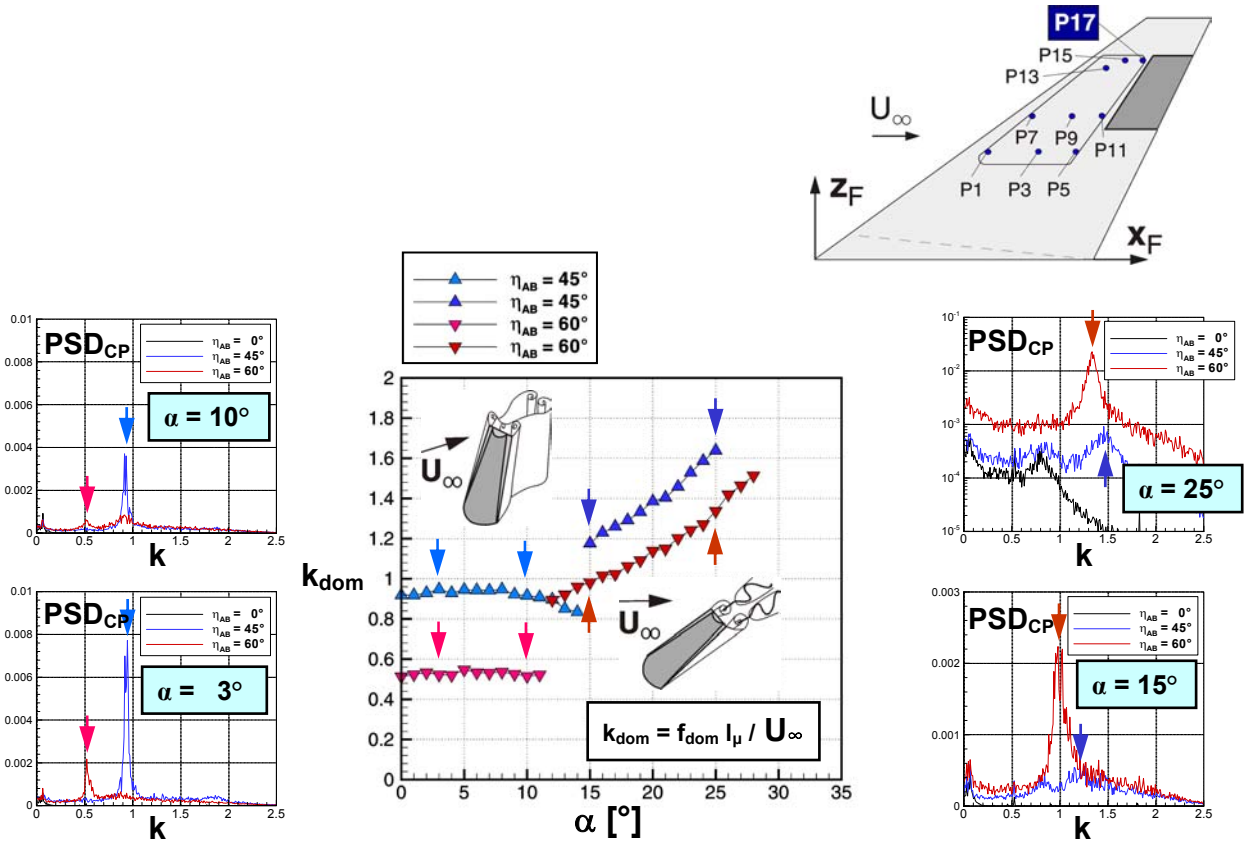

Fig. 15 Power spectral density distributions of fin surface pressures fluctuations PSD_{CP} taken at station P17 and dominant reduced frequencies k_{dom} for airbrake deflections of $\eta_{AB} = 45°$, and 60°; $U_\infty = 40$ m/s, $Re_{l\mu} = 0.97 \times 10^6$.

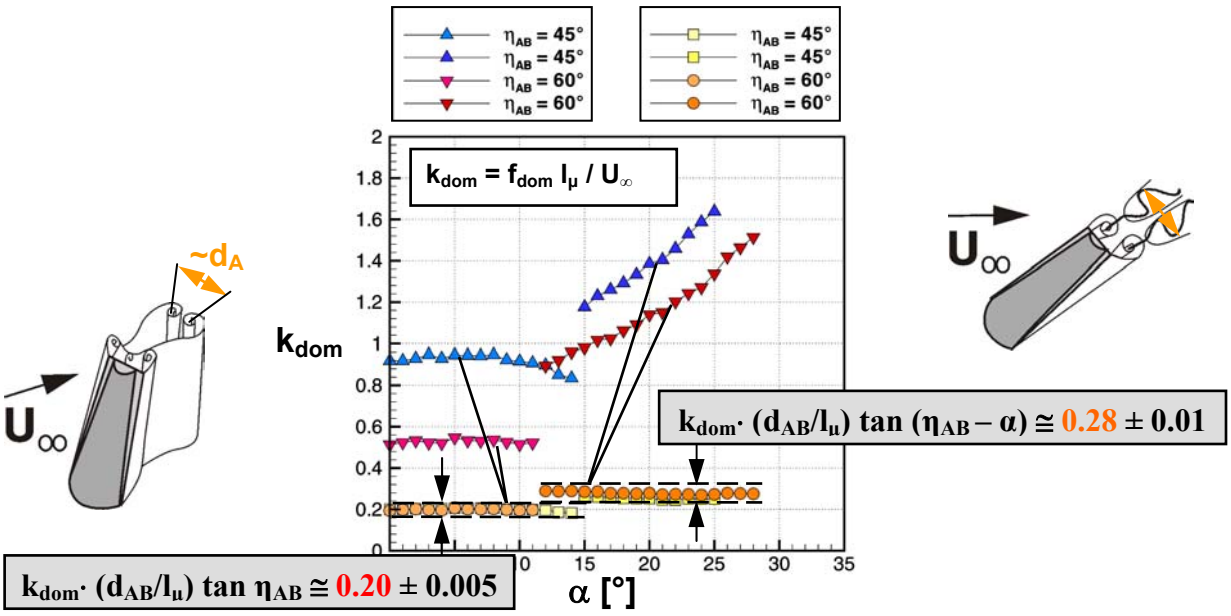

Fig. 16 Scaled dominant reduced buffet frequency k_{dom} as function of angle of attack based on PSD's of fin station P17.

detailed model of a high-agility aircraft of canard-delta wing type fitted with a center-line fin. The airbrake is located upstream at the rear part of the canopy. Compared to the non-deflected case (baseline), the airbrake wake causes unsteady aerodynamic loads on the fin, the levels of which are four to five times higher than those of the baseline. The levels increase with increasing airbrake deflection. Depending on the angle of attack, the surface pressure fluctuations show three characteristic sections: Up to $\alpha \approx 12°$, there is nearly a constant rms level along with a constant reduced frequency due to quasi-periodic vortex shedding creating large-scale coherent structures. From $\alpha \approx 12°$ to $\alpha \approx 25°$, the rms level raises strongly. The dominant reduced frequency of the burst airbrake vortices increases continuously as the effective deflection angle is reduced. Above $\alpha \approx 25°$, the airbrake induced unsteady loads go down to the levels of the baseline. The evolution of large-scale vortices at the airbrake side edges has stopped because the airbrake incidence becomes too small. The unsteady loads are then dominated by the flowfield of the burst wing vortices. The results obtained contribute to setting up a data base for design and evaluation purposes focusing on unsteady aerodynamic loads.

Further analysis will be carried out on the turbulent flow structures and on the scaling of the quantities to extrapolate the results to a full-scale aircraft.

References

[1] Försching H W. *Grundlagen der Aeroelastik*, Springer-Verlag, Berlin, Heidelberg, New York, 1974.

[2] Luber W, Becker J, and Sensburg O. The Impact of Dynamic Loads on the Design of Military Aircraft, *Loads and Requirements for Military Aircraft*, AGARD R-815, AGARD, Neuilly Sur Seine, France 1996, pp. 8-1 – 8-27.

[3] Breitsamter C. *Instationäre Aerodynamik I/II*, Vorlesungsmanuskript, Lehrstuhl für Aerodynamik, Technische Universität München, 2005.

[4] Zimmermann N H, Ferman M A, Yurkovich R N, and Gerstenkorn G. Prediction of Tail Buffet Loads for Design Applications, AIAA Paper 89-1378, April 1989.

[5] Breitsamter C, and Laschka B. Turbulent Flow Structure Associated with Vortex-Induced Fin Buffeting, *Journal of Aircraft*, Vol. 31, No. 4, 1994, pp. 773 – 781.

[6] Breitsamter C. *Turbulente Strömungsstrukturen an Flugzeugkonfigurationen mit Vorderkantenwirbeln*. Dissertation, Technische Universität München, Herbert Utz Verlag Wissenschaft, 1997.

[7] Hummel D. On the Vortex Formation over a Slender Wing at Large Angles of Incidence, *High Angle of Attack Aerodynamics*, AGARD–CP–247, Sandefjord, Norway, Oct. 4–6, 1978, pp. 15-1–15-17.

[8] Hummel D. Effects of Boundary Layer Formation on the Vortical Flow above Slender Delta Wings, *Enhancement of NATO Military Flight Vehicle Performance by Management of Interacting Boundary Layer Transition and Separation*, Prag, Czech Republic, 4–7 Oct 2004.

[9] Hummel D. Untersuchungen über das Aufplatzen der Wirbel an schlanken Deltaflügeln, *Zeitschrift für Flugwissenschaften und Weltraumforschung*, Band 13, 1965, pp. 158–168.

[10] Lambourne N C, and Bryer D W. The bursting of leading edge vortices. Some observations and discussion of the phenomenon, *ARC R & M 3282*, 1962.

[11] Gursul I. Unsteady Flow Phenomena over Delta Wings at High Angle of Attack, *AIAA Journal*, Vol. 32, No. 2, 1994, pp. 225–231.

[12] Gursul I, and Xie W. Buffeting Flows over Delta Wings, *AIAA Journal*, Vol. 37, No. 1, 1999, pp. 58 – 65.

[13] Breitsamter C, and Laschka B. Fin Buffet Pressure Evaluation Based on Measured Flowfield Velocities, *Journal of Aircraft*, Vol. 35, No. 5, 1998, pp.806 – 815.

[14] Ashley H, Rock S M, Digumarthi R V, Chaney K, and Eggers Jr. A J. *Active Control for Fin Buffet Alleviation*, U.S. Air Force Wright Lab., WL-TR-93-3099, Wright-Patterson AFB, OH, Jan. 1994.

[15] Breitsamter C. Aerodynamic Active Control for Fin-Buffet Load Alleviation, *Journal of Aircraft*, Vol. 42, No. 5, 2005, pp. 1252 – 1263.

[16] Roshko A. *On the Development of Turbulent Wakes from Vortex Streets*, NACA Rep. 1191, 1954.

[17] Roshko A. On the wake and drag of bluff bodies, *J. Aeronaut. Sci.*, Vol. 22, 1955, pp. 124 - 132.

[18] Bradbury L. Measurements with a pulsed-wire and a hot-wire anemometer in the highly turbulent wake of a normal plate, *Journal of Fluid Mechanics*, Vol. 77, 1976, pp. 473 – 497.

[19] Ozono S. Flow control of vortex shedding by a short splitter plate asymmetrically arranged downstream of a cylinder, *Physics of Fluids*, Vol. 11, No. 10, 1999, 2928 – 2934.